

C-A/AP/#423

Feb. 2011

The Effects of Realistic Pancake Solenoids on Particle Transport

X. Gu, M. Okamura, A. Pikin, W. Fischer, Y. Luo



**Collider-Accelerator Department
Brookhaven National Laboratory
Upton, NY 11973**

Notice: This document has been authorized by employees of Brookhaven Science Associates, LLC under Contract No.

DE-AC02-98CH10886 with the U.S. Department of Energy. The United States Government retains a non-exclusive, paid-up, irrevocable, world-wide license to publish or reproduce the published form of this document, or allow others to do so, for United States Government purposes.

The Effects of Realistic Pancake Solenoids on Particle Transport

X. Gu, M. Okamura, A. Pikin, W. Fischer, Y. Luo

Corresponding Author: X. Gu

Brookhaven National Laboratory, Upton, NY 11973

Abstract

Solenoids are widely used to transport or focus particle beams. Usually, they are assumed as being ideal solenoids with a high axial-symmetry magnetic field. Using the Vector Field Opera program, we modeled asymmetrical solenoids with realistic geometry defects, caused by finite conductor and current jumpers. Their multipole magnetic components were analyzed with the Fourier fit method; we present some possible optimized methods for them. We also discuss the effects of “realistic” solenoids on low energy particle transport. The finding in this paper may be applicable to some lower energy particle transport system design.

Keywords: realistic solenoids, multipole magnetic fields, particle transport

1. Introduction

Solenoids are used extensively for focusing and transporting the beams in modern accelerators [1-4]. Many high-energy particle detectors are equipped with superconducting (cold) solenoids [5-6], that operate at very low temperatures. Meanwhile, many normal conducting (warm) solenoids [7-10] work at room temperature.

To evaluate the effects of a solenoid on the beam’s parameters, we must calculate the magnetic field [11] or transfer matrix [12-14]. Many researchers discussed ways of assessing magnetic fields, wherein the fields are calculated on-axis [15] or off-axis [16], with an infinite solenoid [17-19], semi-infinite one [20], or a finite one [21-22]. Some papers and textbooks concentrate on calculating the transfer matrix [12-14]. When evaluating either of them, static magnetic fields produced by cold or warm solenoids usually are assumed to be axially symmetric.

Nevertheless, many applications [23-24] require at the least an estimate of the solenoid’s multipole magnetic fields with asymmetry, caused by the realistic solenoid structure. However, very few papers cover this situation.

Moreover, although some effort [23-25] was devoted to ascertaining the magnetic fields of a solenoid’s multipole components, it is important thoroughly to study the origins of these components, and to devise methods of reducing them using the structure of the coil winding.

The pancake-type solenoid is a frequent choice for applications requiring inexpensive high-power density. Their popularity mainly rests on the ability to connect its electricity in series and the water flow in parallel.

In this paper, we address the mechanism that produces multipole magnetic fields in a pancake solenoid and methods to optimize them. Our results demonstrate that the “realistic” solenoid dipole component

is reduced by 180 degrees by rotating the interval pancakes in this solenoid. This finding may be applicable to transporting several species of lower energy, such as electrons [26-28], protons [29] and ions [30-34], or for emittance compensation [23-24, 35] in photocathode electron guns.

We begin with a brief overview of warm solenoid structures, and then analyze the solenoid magnetic fields with different structures. After that, we discuss the effects of one and two “realistic” solenoids on the propagation of particle beams. Finally, some conclusions and recommendations for further study are presented.

2. Structure of the Pancake Solenoid

The multipole magnetic field components of realistic solenoids are caused by their asymmetrical construction, which includes cross over angles, transition angles, pancake polarity, leads, and pancake rotation.

Pancake is the basic element of this kind of solenoid. One warm solenoid is constructed by assembling several pancakes in different combinations. Fig. 1 shows the geometric structure of one pancake.

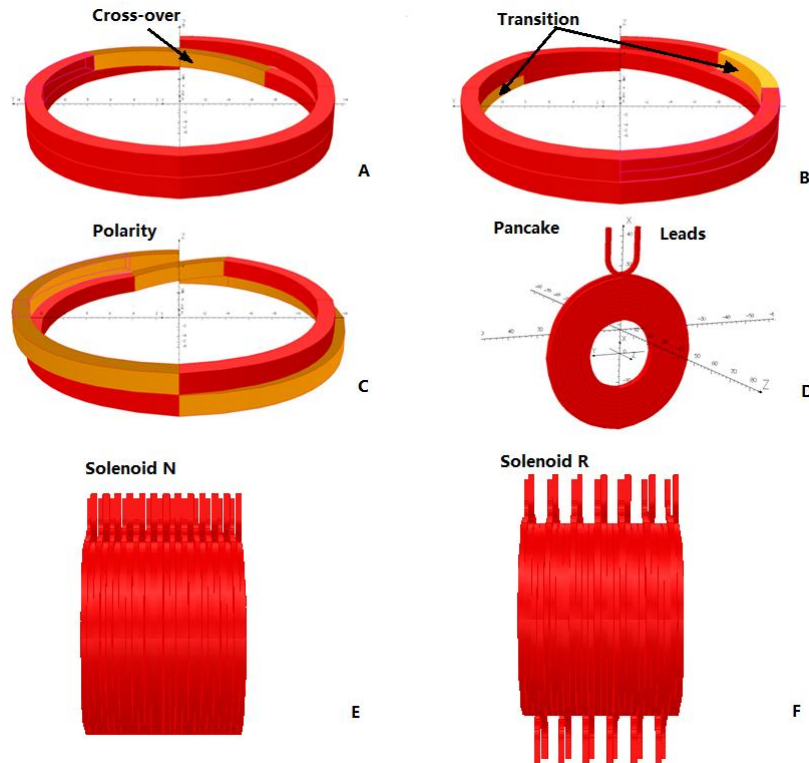


Fig. 1 Structure of a Pancake and Solenoid

One pancake consists of two spirals joined on their inner radius by a cross over (Fig. 1 A). Here, we define the cross over angle as the half angle of the cross over conductor. Fig. 1 A and Fig. 1C have, respectively, a 45° and a 22.5° cross over angle.

Each layer of the pancake's spiral is almost a circle. A transition conductor connects one layer to another one (Fig.1 B). The first inner layer must transit to the second layer before reaching the cross over

conductor. The transition is defined from the transition angle to the cross over angle. The transitions in Fig. 1 B and Fig. 1C, respectively, start from 90° to 45°, and 180° to 22.5°.

Each pancake can have its own polarity. Compared with Fig.1 B, Fig.1 C not only has a different cross over and transition angle, but also has an opposite polarity. After winding several layers, the resulting pancake with leads is illustrated in Fig.1 D.

One solenoid can have many pancakes that may have different polarities or different rotations. The solenoid named Solenoid N has same pancake polarity and rotation direction (Fig. 1 E); the solenoid called Solenoid R, has same pancake polarity but alternate pancake rotation (Fig. 1 F). In this paper, six of 13 pancakes are rotated by 180° alternately in Solenoid R. Solenoids that have same pancake rotation but alternate pancake polarity are named Solenoid P.

Accordingly, the solenoid with different cross over, transition angle, pancake polarity and pancake rotation can have different multipole magnetic field distributions. Furthermore, the leads of individual pancakes may affect these distributions.

3. Analysis Method

Using the different geometric parameters discussed in Section 2, we constructed several realistic solenoids modeling them via Vector Field Opera program. All have thirteen pancakes, each pancake with 10 layers. Their inner- and outer- diameters are 234mm and 526mm, respectively. Their length is 379.6mm. Fig. 2 illustrates the distribution of the longitudinal magnetic field strength of one of them.

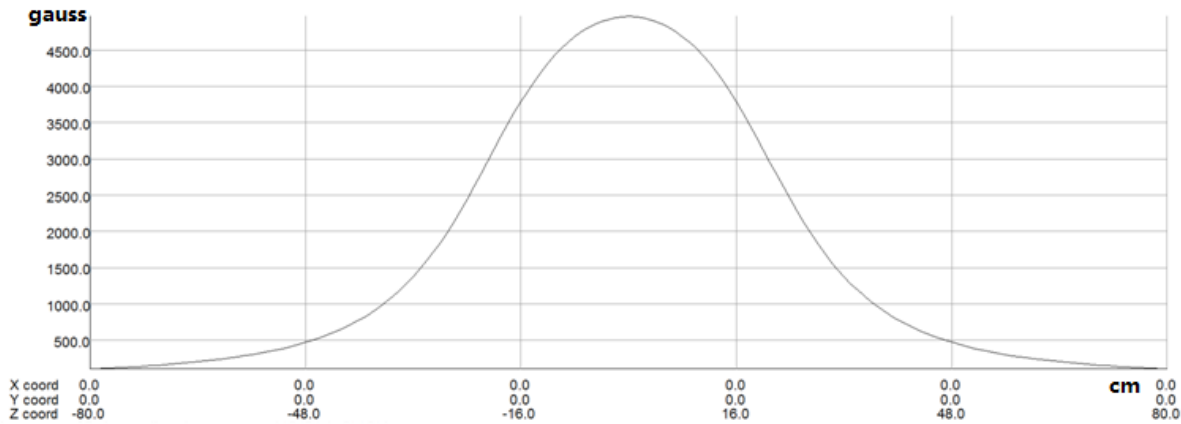


Fig. 2 Solenoid and Its Longitudinal Field Bz

The multipole magnetic field components generated by such “realistic” solenoids are analyzed and compared by Fourier fit method.

In cylindrical coordinates, we can express the radial and azimuthal components of magnetic field B in the form [36-37]:

$$B_r(r, \theta) = \sum_{n=1}^{\infty} (b_n \sin(n\theta) + a_n \cos(n\theta)) \quad (1)$$

$$B_{\theta}(r, \theta) = \sum_{n=1}^{\infty} (b_n \sin(n\theta) - a_n \cos(n\theta)) \quad (2)$$

Where b_n is the amplitudes of the $2n$ pole normal term and a_n is the amplitudes of $2n$ pole skew term in the “European Convention”.

The multipole magnetic field, B_θ can be computed on a reference radius R_{ref} at different longitudinal positions and fitted as Fourier series. Then, according to formula (2), the coefficients of this Fourier series are the multipole magnetic field components. The reference radius $R_{ref} = 75$ mm, and the longitudinal position from -80 cm to +80 cm are used in this paper. The original point of cylindrical coordinate was set at the center of the solenoid’s geometry.

4. Multipole Components for Different Solenoid Structures

In this section, we calculate the normalized multipole magnetic field components for different solenoid structures. They are the solenoids with different leads, transition angles, cross over angles, pancake rotations and pancake polarities.

Figure 3 shows the multipole components for solenoids with and without leads.

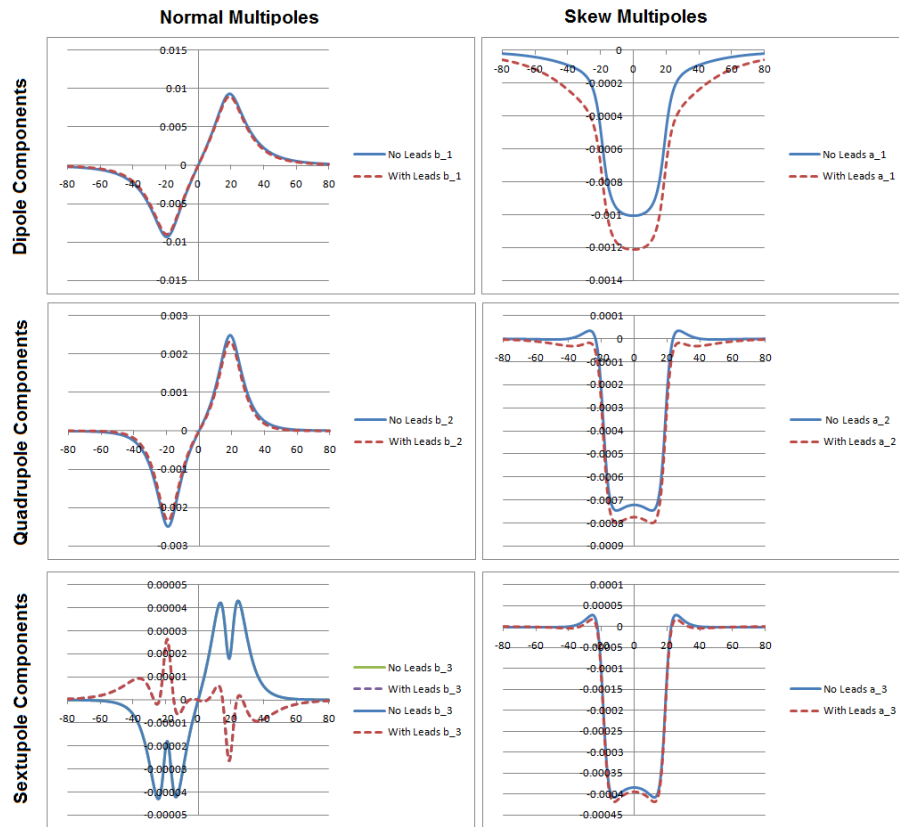


Fig. 3 Solenoids Multipole Components with and without Leads

In Fig. 3, the three rows respectively represent the dipole, qaudrupole, and sextupole components; the two columns represent the normal (left) and skew (right) multipole components. The horizontal axis is the longitudinal position in units of centimeters and the vertical axis is the normalized amplitudes of the multipole component. Because the multipole components with $n > 3$ have lower magnetic field strength, only those with $n \leq 3$ are shown.

As evident from Fig. 3, the distribution of multipole component ($n \leq 3$) with and without leads have only a slight difference except for the normal sextupole magnetic field. For this reason, in further analyses we removed the leads from the models.

Figure 4 plots the calculated solenoid multipole components with different transition angles.

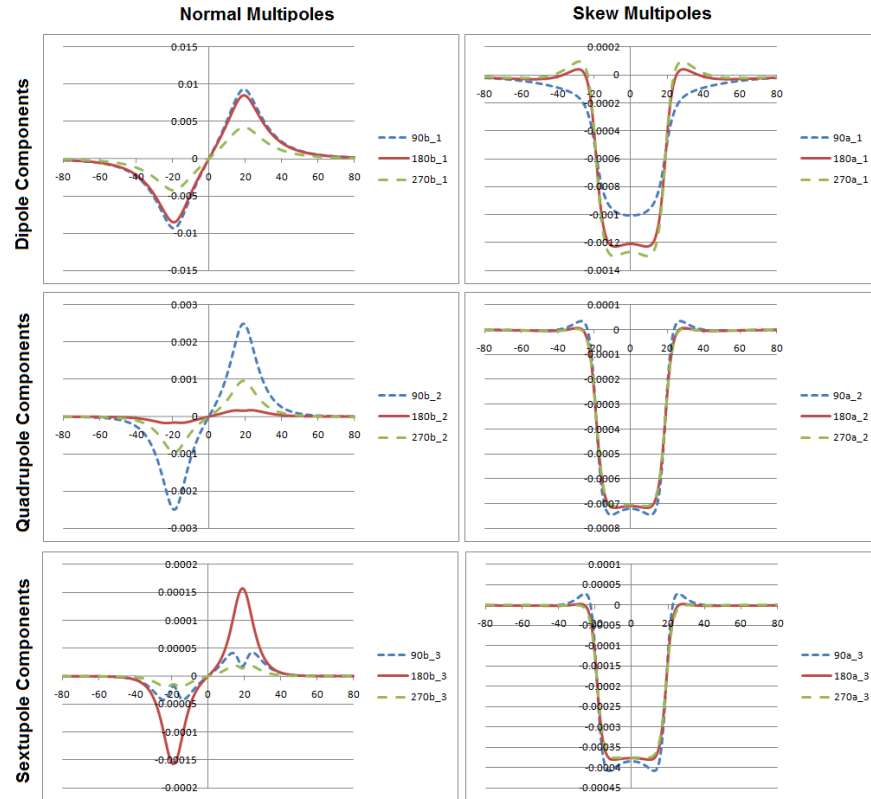


Fig. 4 Solenoids Multipole Components versus Transition Angles

With the same cross over angle (22.5°), we studied three solenoid structures with 90° , 180° and 270° transition angles. Fig. 4 reveals that different transition angles induce different distributions of high order component. Seemingly, the solenoid with the 270° angle has the minimum normal dipole component, while the solenoid with the 180° angle has the minimum normal quadrupole component.

The multipole components of solenoids with different cross over angles were computed and are plotted in Fig. 5.

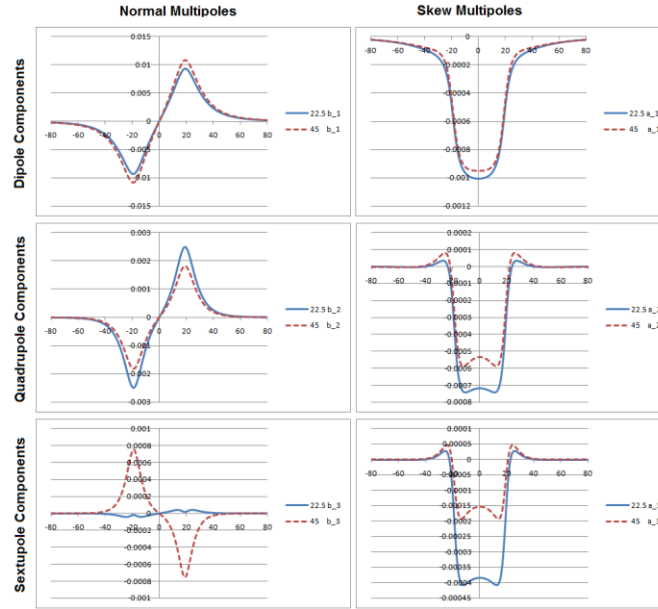


Fig. 5 Solenoids Multipole Components versus Cross over Angle

In this instance, we changed the cross over angle from 22.5° to 45° and transition angle is 90° . Because conductor transits from the transition angle to the cross over angle, the length of transition conductor also changes. The effects of the cross over angle on multipole components are unclear.

Figure 6 plots the calculated multipole components of solenoids with (Solenoid R) and without (Solenoid N) pancake rotation. The transition is set to 270° and the cross over angle is 22.5° .

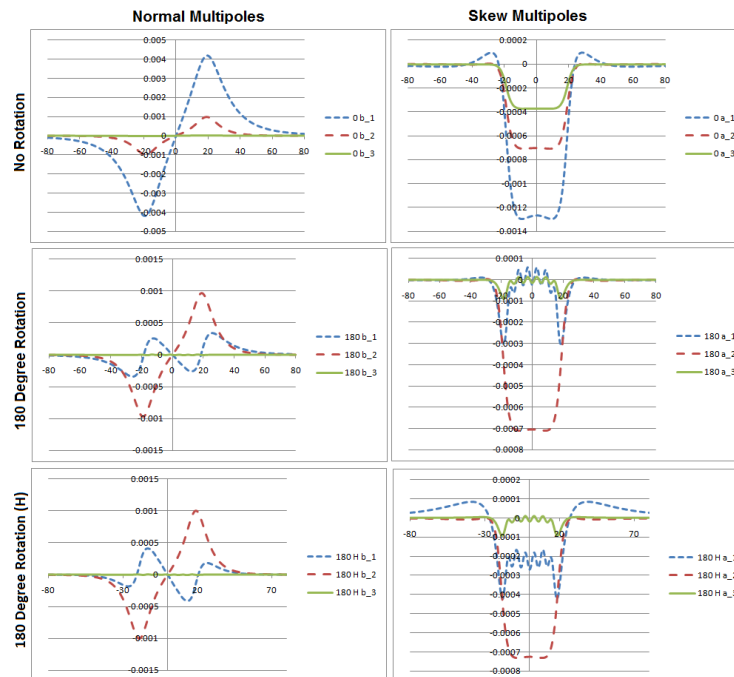


Fig. 6 180° Rotation versus no Rotation

123

124 In Fig. 6, b (a) _1, b (a) _2 and b (a) _3 correspond, respectively, to normal (skew) dipole, quadrupole
125 and sextupole components. The first row is calculated with Solenoid N and the second with Solenoid R.

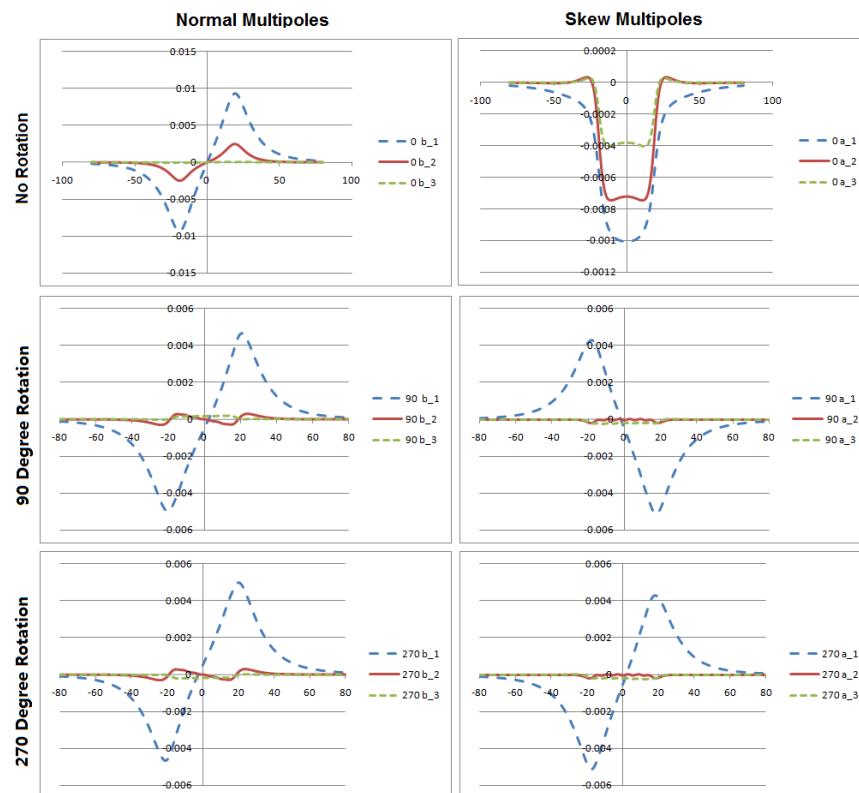
126 From second row in Fig. 6, we conclude that the 180° alternate rotation of pancakes in a normal
127 solenoid reduces the normal dipole component dramatically. This result is confirmed by the solenoid
128 with the 180° transition angle and 22.5° cross over angle. However, apparently it does not change the
129 normal qadrupole and sextupole components.

130 Nevertheless, for Solenoid R, it is difficult to assemble a coil with output wires pointing in opposite
131 directions. Besides, there should be some jumpers connecting these coils in series, and they also will
132 introduce some multiple components.

133 To resolve this problem, we changed the layers of seven non-rotated pancakes in Solenoid R from 10 to
134 9.5, so that all pancakes have the same azimuthal position. The simulation for this configuration is
135 shown as the third row in Fig. 6.

136 The normal dipole component can be reduced by using Solenoid R with a 180° rotation. The quadrupole
137 component can be optimized by 90° pancake rotation or 270° rotation; in this instance, the transition
138 angle is set to 90° and the cross over angle is 22.5°.

139 From Fig. 7, we note a reduction in both the normal quadrupole component and normal dipole
140 component. The skew quadrupole component also decreases, but the skew dipole component increases.



141

142

Fig. 7 Optimization of the Quadrupole Component

Finally, the components of the solenoid multipole magnetic field with (Solenoid P) and without (Solenoid N) polarity pancakes, were assessed and are presented in Fig. 8.

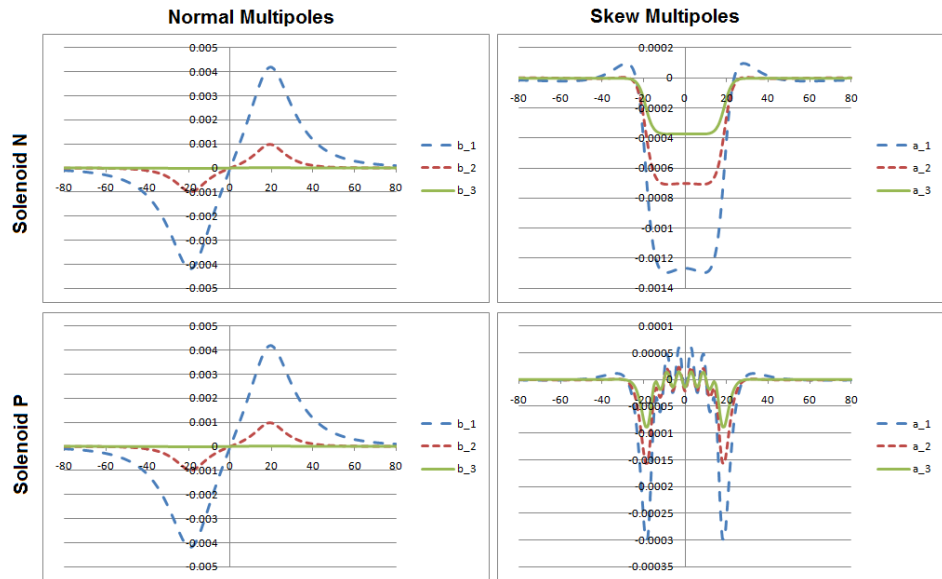


Fig. 8 No Polarity versus with Polarity

This figure shows that in Solenoid P only the skew multipole components change; the normal multipole components do not.

According to different design requirements, we can optimize the normal dipole, quadrupole, and sextupole components and skew the dipole components by using different transition angles; thereafter further optimization is achieved different pancake rotation.

5. Beam Transport with a Realistic Solenoid

In this section, firstly, we discuss the detrimental effects of a single realistic solenoid on particle transport. Then we analyze the effects of two realistic solenoids on propagation of a particle beam.

The dipole component's field of a single realistic solenoid can deflect some kinds of particle trajectories at low energy. To verify this effect and find methods to improve it, we simulated the passage of some particles through a single Solenoid N and Solenoid R. These solenoids have the same dimensions, with a 180° transition angle and a 22.5° cross over angle.

Table 1 Position Change for Different Particles

Particle	Atomic Number	Charge	Energy (kV)
Proton	-	+1	80
H	1	-1	50
He	2	+1	13
C	6	+5	102
Ne	10	+2	22
Si	14	+13	238
Fe	26	+20	442

The center of solenoid is set at $Z=0$, and their axis is oriented along the Z -axis. All particles start from $Z=-25$ cm on the solenoid axis. Table 1 lists the particle's parameters; their trajectories are illustrated in Fig. 9.

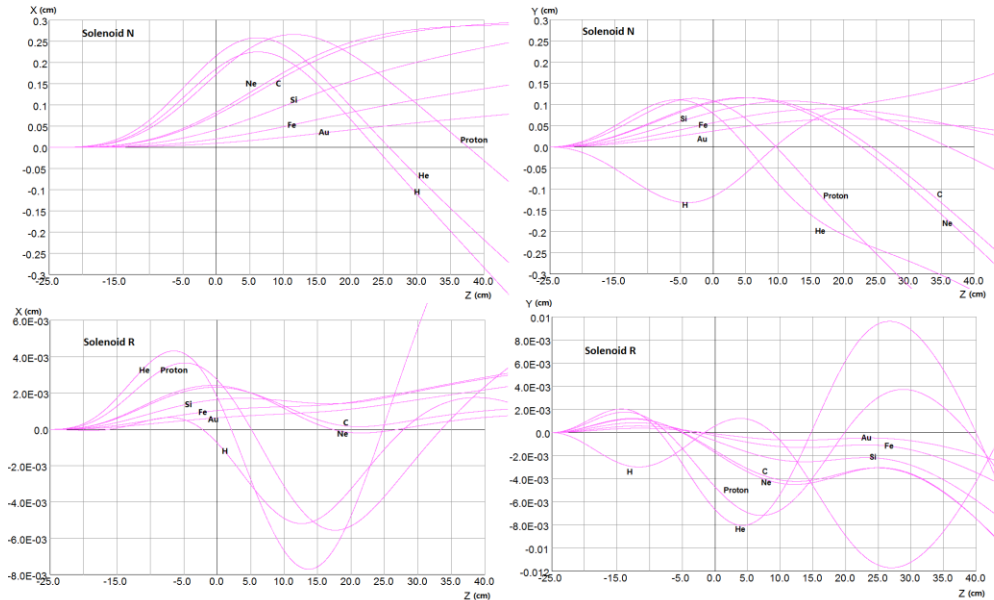


Fig. 9 Particle Trajectories with Normal and Rotated Solenoid

As Fig. 9 reveals, unlike the ideal solenoid, the particle's trajectories do not follow along the center axis when they pass through these realistic solenoids. From -25 cm to 40 cm, the particle trajectories of Solenoid R have at least 10 times smaller deviations in transverse amplitude than do those of Solenoid N.

Sometimes, the beam transport system has several contiguous solenoids. We discuss the effects of relative solenoid orientation on beam propagation for Cases A and Case B in Fig. 10 that have only two adjacent realistic solenoids.

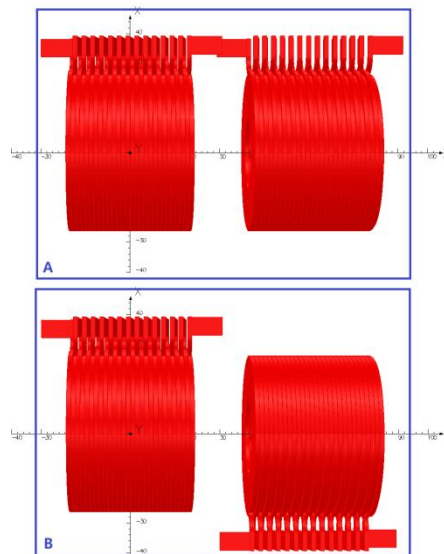


Fig. 10 Arrangement of the Two Solenoids

For Cases A and B, we use two kinds of solenoids, Solenoid N and Solenoid R; their configurations are termed Case A-N, Case A-R, Case B-N, and Case B-R, respectively. The center of left solenoid is set to $Z=0$, another solenoid's center is set to $Z= 60$ cm. In the simulations, a single electron starts from $Z=0$, and its velocity is parallel to the solenoid's axis. The simulated trajectories for these four cases are shown in Fig. 11.

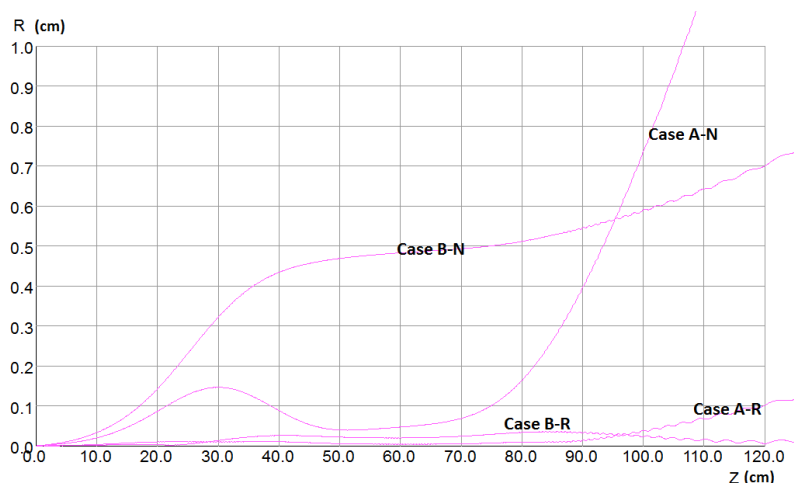


Fig. 11 Trajectories for Different Solenoid Arrangements

As depicted, Case B undergoes less angle change after passing through two solenoids than Case A; while for both cases with Solenoid R, there is less change in angle and position than Solenoid N. Thus, when designing a low energy beam transport system with solenoids, different beam requirements may necessitate different solenoid configurations.

6. Discussion

In this paper, we presented some simulations with realistic solenoids and their affects on the transport of low energy particle beam. Unlike the ideal solenoids, the realistic solenoids have high order components that can deflect particle's trajectories. With the 180° alternate rotation of pancakes in the normal solenoids, the normal dipole component can be reduced dramatically. Using these solenoids (Solenoid R), we can design a low energy particle's transport system with less angle and position deviation. Combined with the transfer maps [39], which include high order multipole field, these simulations also can help us in understanding the particle's trajectories when they pass the realistic solenoids.

However, there are more researches are needed on this topic. Firstly, the effects of cross over angles are not very clear. Secondly, because there is a force placed on wire when winding the pancakes, the final realistic transition angle and cross over angle may differ from their design value. This force may distort them, and introduce more complex conductor geometry in pancakes. More research also is needed on quadrupole and sextupole effects.

7. Acknowledgment

The authors acknowledge helpful discussions with Walter Shaffer and Jonathan Hock.

References

- [1] A. Yamamoto, Y. Makida, R. Ruber, et al., Nucl. Instr. and Meth. A 584 (2008) 53 – 74.
- [2] S.H. Aronson, J. Bowers, J. Chiba, et al., Nucl. Instr. and Meth. A 499 (2003) 480 – 488.
- [3] S. Seletskiy, in: Proceedings of PAC07, Albuquerque, New Mexico, 2007, pp: 3109 – 3111.
- [4] A.A. Efremov, E.K. Koshurnikov, Y.Y. Lobanov, et al., Nucl. Instr. and Meth. A 585 (2008) 182 – 200.
- [5] L. Mirabito, Nucl. Instr. and Meth. A (2010), doi:10.1016/j.nima.2010.02.243
- [6] D. Toprek, Y. Nosochkov, Nucl. Instr. and Meth. A 612 (2010) 260 – 273.
- [7] S.J. Russell, Z.-F. Wang, W.B. Haynes, Phys. Rev. ST Accel. Beams. 8 (2005) 080401.
- [8] R.J. Hayden, M.J. Jakobson, Nucl. Instr. and Meth. A 278 (1989) 394 – 396.
- [9] S. M'Garrech, Nucl. Instr. and Meth. A 550 (2005) 535 – 542.
- [10] E. Beebe, J. Alessi, S. Bellavia, et al., Rev. Sci. Instrum. 71 (2000) 893 – 895.
- [11] D. B. Montgomery, Solenoid Magnet Design, John Wiley & Sons, Inc. New York, 1969.
- [12] G. Xu, Phys. Rev. ST Accel. Beams. 7 (2004) 044001.
- [13] D. Rubin, in: Alexander Wu Chao and Maury Tigner (Eds.), Handbook of Accelerator Physics and Engineering, 2nd ed., World Scientific Publishing Co. Pte. Ltd. Singapore, 2002, pp.272 – 277.
- [14] G. Franchetti, Phys. Rev. ST Accel. Beams. 4 (2001) 074001.
- [15] C. Chia and Y. Wang, Phys. Teach. 40 (2002) 288 – 289.
- [16] R. H. Jackson, IEEE Trans. Electron Devices 46 (1999) 1050 – 1062.
- [27] V. Labinac, N. Erceg, D. Kotnik-Karuza, Am. J. Phys. 74 (2006) 621-627.
- [18] O. Espinosa and V. Slusarenko, Am. J. Phys. 71 (2003) 953 – 954.
- [19] K. Fillmore, Am. J. Phys. 53 (1985) 782–783.
- [20] G. V. Brown and L. Flax, J. Appl. Phys. 35 (1964) 1764–1767.
- [21] J. Farley and R.H. Price, Am. J. Phys. 69(2001) 751 – 754.

- 227 [22] V. I. Danilov, M. Ianovic, Nucl. Instr. and Meth. 94 (1971) 541 – 550.
- 228 [23] M. Ferrario, M. Migliorati, P. Musumeci, et al., in: Proceedings of EPAC 2006, Edinburgh, Scotland,
229 2006, pp. 169 - 171.
- 230 [24] J. Schmerge, LCLS Gun Solenoid Design Considerations (LCLS-TN-05-14), LCLS project, SLAC, 2005.
- 231 [25] A. Wolski, M. Venturini, in: Proceedings of EPAC2004, Lucerne, Switzerland, 2004, pp: 2185 – 2187.
- 232 [26] V. Shiltsev, K. Bishofberger, V. Kamedzhiev, et al., Phys. Rev. ST Accel. Beams. 11 (2008) 103501.
- 233 [27] D. Xiang, Y.C. Du, L.X. Yan, et al., Phys. Rev. ST Accel. Beams. 12 (2009) 022801.
- 234 [28] W. Fischer, Y. Luo, A. Pikin, etc, in: Proceedings of IPAC10, Kyoto, Japan, pp: 513 – 515.
- 235 [29] G. Ciavola, L. Celona, S. Gammino, et al., in: Proceedings of LINAC2002, Gyeongju, Korea, 2002, pp:
236 674 – 676.
- 237 [30] E. Lee, Nucl. Instr. and Meth. A 544 (2005) 187 – 193.
- 238 [31] R. Hollinger, P. Spädtke, Rev. Sci. Instrum. 79 (2008) 02B704.
- 239 [32] J. Alessi, D. Barton, E. Beebe, et al., in: Proceedings of LINAC2006, Knoxville, Tennessee, USA, 2006,
240 pp: 385 – 387.
- 241 [33] M. Eshraqi, G. Franchetti, A.M. Lombardi, et al., Phys. Rev. ST Accel. Beams. 12 (2009) 024201.
- 242 [34] J.H. Li , J.Y. Tang, Nucl. Instr. and Meth. A 574 (2007) 221 – 225.
- 243 [35] J.B Rosenzweig, A.M Cook, M.P. Dunning, et al., in: Proceedings of 2005 Particle Accelerator
244 Conference, Knoxville, Tennessee, 2005, pp. 2624 – 2626.
- 245 [36] A. K. Jain, in: Turner, S [ed], CAS - CERN Accelerator School : Measurement and Alignment of
246 Accelerator and Detector Magnets, Geneva, CERN, 1998, pp. 1 – 26.
- 247 [37] A. K Jain, P. Wanderer, in: Alexander Wu Chao and Maury Tigner (Eds.), Handbook of Accelerator
248 Physics and Engineering, 2nd ed., World Scientific Publishing Co. Pte. Ltd. Singapore, 2002, pp.409 – 414.
- 249 [38] J. Back, J.Pozimski,P. Savage, et al, in: Proceedings of IPAC10, Kyoto, Japan, pp: 648 – 650.
- 250 [39] C. E. Mitchell and A. J. Dragt, Phys. Rev. ST Accel. Beams. 13 (2010) 064001.